Synthesis and characterization of Ga_2O_3 nanosheets on 3C-SiC-on-Si by low pressure chemical vapor deposition

Subrina Rafique, Lu Han, Jaesung Lee, Xu-Qian Zheng, Christian A. Zorman, Philip X.-L. Feng, and Hongping Zhao

Citation: J. Vac. Sci. Technol. B **35**, 011208 (2017); doi: 10.1116/1.4974158
View online: http://dx.doi.org/10.1116/1.4974158
View Table of Contents: http://avs.scitation.org/toc/jvb/35/1
Published by the American Vacuum Society

Synthesis and characterization of Ga_2O_3 nanosheets on 3C-SiC-on-Si by low pressure chemical vapor deposition

Subrina Rafique,[a] Lu Han, Jaesung Lee, Xu-Qian Zheng, Christian A. Zorman, Philip X.-L. Feng, and Hongping Zhao[b]
Department of Electrical Engineering and Computer Science, Case Western Reserve University, Cleveland, Ohio 44106

(Received 3 November 2016; accepted 4 January 2017; published 12 January 2017)

This study presents the synthesis of single crystalline β-Ga_2O_3 nanosheets on SiC by low pressure chemical vapor deposition. High purity gallium (Ga) metal and oxygen as source materials and argon as carrier gas were utilized for the synthesis of the nanosheets on a 3C-SiC-on-Si substrate. These single-crystal Ga_2O_3 nanosheets are free-standing 2D extrusions from their 1D rods, typically 1.5–7 μm in lateral size and 20–140 nm in thickness, featuring aspect ratios ranging from ~10 to 350. Structural studies based on transmission electron microscopy and Raman spectroscopy revealed the monoclinic phase of Ga_2O_3 with a single crystalline nature. High resolution transmission electron microscopy with a selected area electron diffraction pattern recorded on a single β-Ga_2O_3 nanosheet further confirmed their single crystalline nature, with a growth direction perpendicular to (111) crystallographic plane. The growth process governing the formation of these nanosheets is a vapor-solid growth mechanism since no metal catalyst was used. These β-Ga_2O_3 nanosheets exhibit new possibilities and potential for future functional nanodevices that would benefit from their extremely large surface area to volume ratios. © *2017 American Vacuum Society*. [http://dx.doi.org/10.1116/1.4974158]

I. INTRODUCTION

Gallium oxide (Ga_2O_3) is an emerging ultrawide bandgap semiconductor with a room temperature bandgap of ~4.9 eV.[1–7] It possesses outstanding chemical and thermal stability up to 1400 °C (Refs. 1 and 8) and has high transparency in the deep ultraviolet and visible wavelength regions. Compared to other known wide bandgap semiconductor materials, it has a breakdown voltage of ~8 MV/cm, even higher than those of GaN (3.3 MV/cm) and SiC (2.5 MV/cm) which are currently being used for high power device applications. Thermodynamically stable β-Ga_2O_3 nanostructures such as nanowires,[9] nanorods,[10] nanoribbons,[11] nanobelts,[12] and nanosheets[13] have been synthesized by several vapor phase deposition techniques using different types of growth substrates, metal catalysts, and precursors.

One dimensional (1D) and two dimensional (2D) nanostructures have attracted much attention as they are excellent candidates to investigate the dependence of optical, electrical, and magnetic properties on quantum confinement effect and morphology of the nanostructure.[14,15] They are also useful for studying dimensionality confined transport phenomena.[16] Therefore, morphology controlled synthesis of nanostructures is important because their chemical and physical properties depend on their dimensionality, size, and shape. In particular, nanosheets offer particularly interesting opportunities for realizing novel functional nanostructures in electromechanical, optical, and electronic devices due to their extreme aspect ratios and high surface area-to-volume ratios as compared with other common nanostructures.

The synthesis of nanomaterials usually falls within two well established growth mechanisms: (1) vapor–liquid–solid (VLS) and (2) vapor–solid (VS). In the VLS growth mechanism, a foreign metal catalyst is used to initiate the nucleation of the nanomaterials. However, the catalyst can introduce undesired impurities in the nanomaterials that can be detrimental to device performance.[17,18] To avoid undesired impurities, catalyst-free or self-catalytic synthesis of nanomaterial is necessary. There are very few reports in the literature that describe Ga_2O_3 nanomaterials synthesized by self-catalytic or catalyst-free methods.[1,19–22] Very recently, however, we reported the self-catalytic growth of Ga_2O_3 nanorods on 3C-SiC-on-Si substrates.[23]

SiC is a well-known wide bandgap semiconductor material that has many polytypes. Among them, 3C-SiC is the only polytype with a cubic crystal structure, which permits inversion at low electric field strength.[24] It also has isotropic and higher electron Hall mobility as compared to the other polytypes of SiC. Its high breakdown electric field, high melting temperature and affinity to hydrocarbon makes it an interesting candidate for high temperature gas sensing. Since Ga_2O_3 based sensors can also operate at high temperature, SiC is well suited as a substrate for such Ga_2O_3 based devices because of its stability at high temperature. Furthermore, as a semiconducting material, 3C-SiC provides the advantage of directly realizing vertically structured devices without the need of transferring the synthesized materials to other conducting substrates.

In this paper, we report the synthesis of 2D β-Ga_2O_3 nanosheets grown on 3C-SiC-on-Si substrates by low pressure chemical vapor deposition (LPCVD). The crystal structure and morphology of the as-synthesized nanosheets are investigated. Structural studies reveal the single crystalline

[a]Electronic mail: subrina.rafique@case.edu
[b]Electronic mail: hongping.zhao@case.edu

nature of the nanosheets. Furthermore, a possible growth mechanism of the freely suspended nanosheets is proposed. These β-Ga_2O_3 nanosheets are promising candidates as building blocks for future functional nanodevices.

II. EXPERIMENTAL DETAILS

The β-Ga_2O_3 nanosheets were synthesized using a conventional tube furnace with a programmable temperature controller. A 0.5 μm-thick, 3C-SiC film that was heteroepitaxially grown on a (100) Si wafer by atmospheric pressure chemical vapor deposition was used as the substrate for Ga_2O_3 growth.[25] High purity gallium pellets (Alfa Aesar, 99.99999%) and oxygen were used as the source materials and argon was used as carrier gas. The growth temperature varied between 780 and 950 °C. The growth was conducted for 40 min with a flow of 5 sccm of oxygen and 300 sccm of argon. The growth pressure was 3 Torr.

The structure and morphology of the Ga_2O_3 nanosheets were characterized using field emission scanning electron microscopy (FESEM), atomic force microscopy (AFM), transmission electron microscopy (TEM), and Raman spectroscopy. FESEM images were taken with an FEI Helios 650. AFM measurements were conducted with an Agilent 5500 AFM. To carry out the AFM measurements, the Ga_2O_3 nanosheets were transferred on a SiO_2/Si substrate using thermal release tape. High resolution transmission electron microscopy (HRTEM) images and selected-area electron diffraction (SAED) were taken with an FEI Tecnai F30 at 300 kV. The TEM sample was prepared by dispersing the Ga_2O_3 nanosheets in ethanol and then transferring them to a Cu grid covered with carbon film. The Raman spectrum was taken at room temperature using a 532 nm laser at a power of 300 μW. The beam was focused using a 100× microscope objective and typical spot size was ~1 μm.

III. RESULTS AND DISCUSSION

The experimental investigations indicate that both the growth substrate and the catalyst influence the morphology of nanomaterials grown on foreign substrates. Here, we compare the growth of Ga_2O_3 nanostructures on two different substrates: (1) 3C-SiC-on-Si (with and without a catalyst) and (2) SiO_2-on-Si without a catalyst. Figure 1 shows the FESEM [(a) and (b)] and SEM (c) images of the grown nanomaterials. The growth temperature was 780 °C and the growth was conducted for 20 min. On the 3C-SiC-on-Si substrate with a 0.5 nm thick Au catalyst [Fig. 1(a)], high-density arrays of thin and long (~tens of micrometers) Ga_2O_3 nanobelts were grown. The inset high resolution FESEM image revealed that the surface of the Ga_2O_3 nanobelts has grovelike morphologies. Ga_2O_3 nanomaterials were also synthesized on other substrates with Au catalyst such as sapphire, SiO_2-on-Si, GaN, and Si (images not shown). We found that the grown materials have similar morphologies irrespective of the growth substrate. Under the same growth condition, flat Ga_2O_3 nanosheets originating from the sidewalls of Ga_2O_3 nanorods were formed on the 3C-SiC-on-Si substrate without a catalyst as shown in Fig. 1(b). In contrast, on the amorphous SiO_2-on-Si substrate without a catalyst, randomly oriented Ga_2O_3 nanorods were grown as shown in Fig. 1(c). From the morphological differences for the Ga_2O_3 nanostructures grown on different substrates, we believe that both substrate and catalyst play an important role during the Ga_2O_3 nanostructure growth. The lattice and crystal symmetry mismatch between the substrate and the nanostructures are responsible for the morphological differences in case of catalyst free growth.

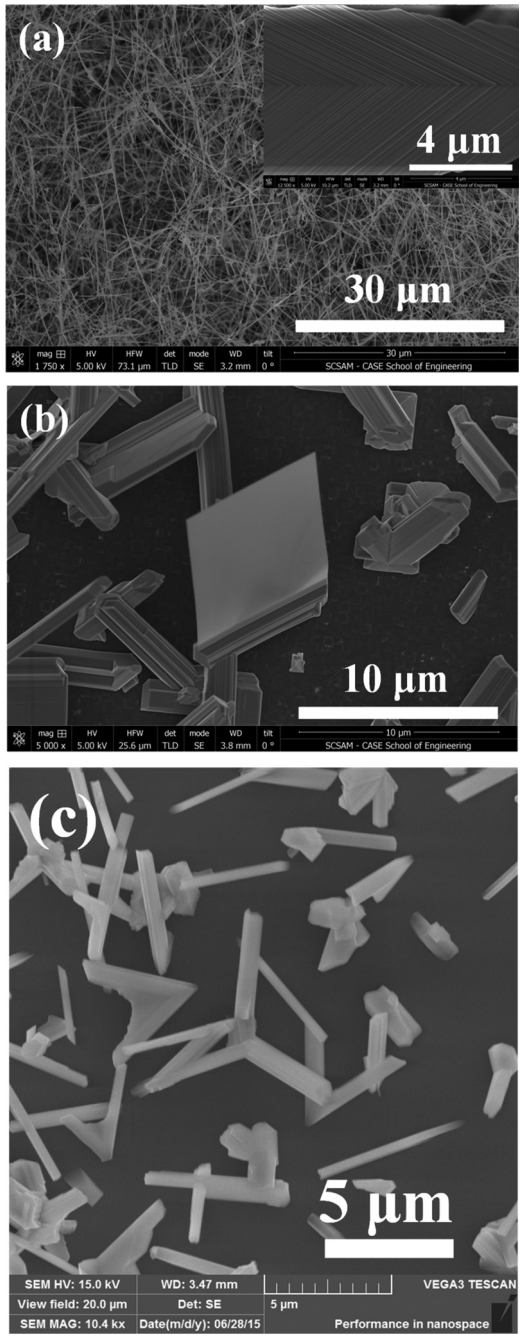

FIG. 1. Top view FESEM and SEM images of grown Ga_2O_3 nanomaterials on: (a) a 3C-SiC-on-Si substrate with a 0.5 nm-thick Au catalyst layer; (b) a 3C-SiC-on-Si substrate without a catalyst; and (c) a SiO_2-on-Si substrate without a catalyst under the same growth conditions. Insets show high magnification top view FESEM and SEM images of the Ga_2O_3 nanomaterials.

To further characterize the morphology of the as-grown Ga_2O_3 nanosheets, FESEM was conducted. Top view FESEM

images revealing the general morphology of the Ga_2O_3 nanosheets are shown in Fig. 2. The nanosheets originating from the sidewalls of the nanorods can be seen in the high magnification FESEM image of Fig. 2(b). The nanosheets have a rectangular geometric shape with straight edges and sharp corners. Based on the statistical measurements of the SEM images, these structures have a width between 1.5 and 7 μm and thickness between ~20 and 140 nm. The thicknesses of the Ga_2O_3 nanosheets were further confirmed by AFM. The nanosheets were transferred on a substrate with prefabricated holes both for the AFM measurement and for evaluating their mechanical properties. Figure 3(b) shows an example of an AFM step-height profile for a typical Ga_2O_3 nanosheet transferred onto a SiO_2-on-Si substrate. The nanosheet has a thickness of ~44 nm.

Figure 4 shows the schematic illustration of the proposed growth mechanism of β-Ga_2O_3 nanosheets on 3C-SiC-on-Si substrates by LPCVD. Since no metal catalyst was used for the synthesis, the growth followed the VS growth mechanism. Ga vapor generated from the precursor material at high temperature was transported to the substrate by the carrier gas and was adsorbed at suitable substrate surface sites where the Gibbs free energy is a minimum. These individual adatoms then diffused along the substrate surface and bound to each other. The reaction between the bound atoms with the oxygen gas precursor present in the growth chamber resulted in the nucleation of Ga_2O_3 droplets. Subsequently, supersaturation of the droplets led to the formation of Ga_2O_3 nanorods. Previously, we have reported the synthesis of β-Ga_2O_3 thin films on sapphire substrates.[2,4] The close

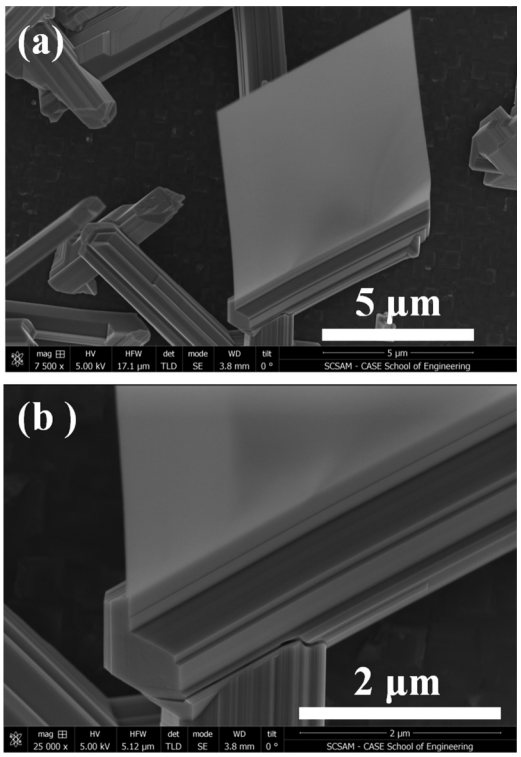

FIG. 2. (a)–(b) Top view FESEM image of a Ga_2O_3 nanosheet synthesized on a 3C-SiC-on-Si substrate.

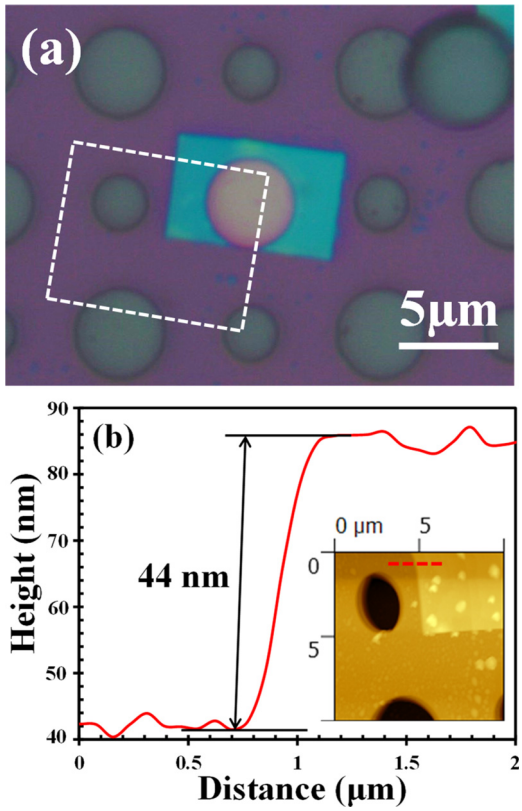

FIG. 3. (Color online) (a) Optical image of a single Ga_2O_3 nanosheet transferred onto a SiO_2-on-Si substrate. (b) AFM height profile of the transferred Ga_2O_3 nanosheet. The inset shows an AFM image of the nanosheet.

lattice match and crystal symmetry between β-Ga_2O_3 and sapphire promoted the uniform thin film growth. However, the crystal structure of 3C-SiC (zinc blende) is quite different from β-Ga_2O_3 (monoclinic). Such crystal asymmetry

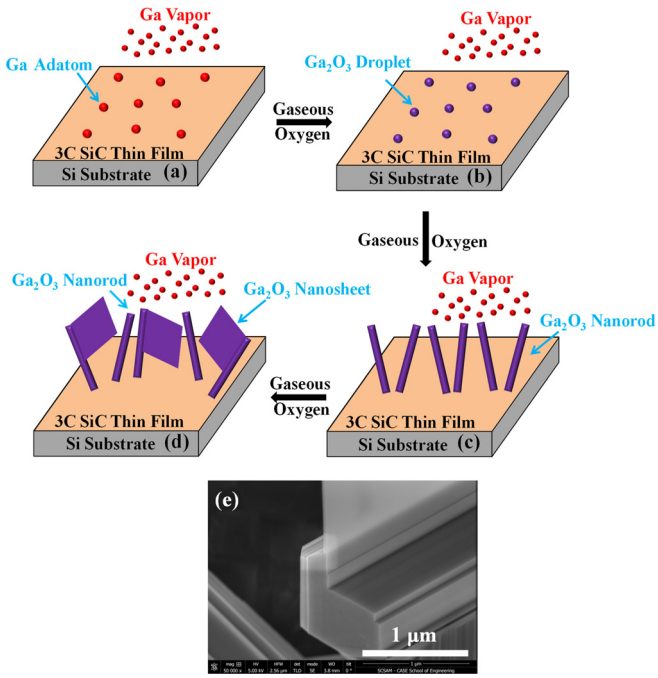

FIG. 4. (Color online) (a)–(d) Schematics of the proposed growth mechanism for Ga_2O_3 nanosheets. (e) Top view FESEM image showing the nucleation site of a Ga_2O_3 nanosheet synthesized on a 3C-SiC-on-Si substrate.

provided the nucleation sites along with sufficient surface energy for the 1D Ga_2O_3 nanorods to grow on 3C-SiC-on-Si. As can be seen from the FESEM image of Fig. 4(e), the nanosheets originated from the sidewalls of the rods. This can be due to the formation of secondary nucleation sites on the sidewalls of previously grown nanorods which have the lowest Gibbs free energy. These nucleation sites formed due to the condensation of continuously supplied gallium and acted as the nucleation centers for the growth of the nanosheets. The nanosheets followed the same growth mechanism as the nanorods. AFM measurements revealed that the nanosheets become thinner and taper as they extend away from the nanorods which further corroborated our proposed growth mechanism for the nanosheets. The proposed growth mechanism of Ga_2O_3 nanosheets is different from the previously reported growth mechanism of free standing ZnO 2D nanomembranes from the sidewalls of ZnO 1D nanowires.[26]

The crystal structure and morphology of the Ga_2O_3 nanosheets were further investigated in detail by TEM and HRTEM as well as SAED patterns. Figure 5(a) shows the TEM image of a single Ga_2O_3 nanosheet having a uniform width of ~1.6 μm along its entire length of ~6 μm. The SAED pattern [inset of Fig. 5(c)] taken along the [10–1] zone axis reveals that the synthesized nanosheets are single crystalline β-Ga_2O_3. The lattice fringes are clearly visible in the HRTEM images of Figs. 5(b) and 5(c). From Fig. 5(c), the resolved lattice fringes have an interplanar spacing of 0.25 nm, which corresponds to monoclinic β-Ga_2O_3 (111) planes.[27] The nanosheet growth direction is indicated by an arrow in Fig. 5(c) which is perpendicular to the (111) crystallographic plane. Moreover, from the HRTEM images shown in Fig. 5(b), no obvious defects such as dislocations or stacking faults are observed; further demonstrating high quality and single crystalline nature of the nanosheets.

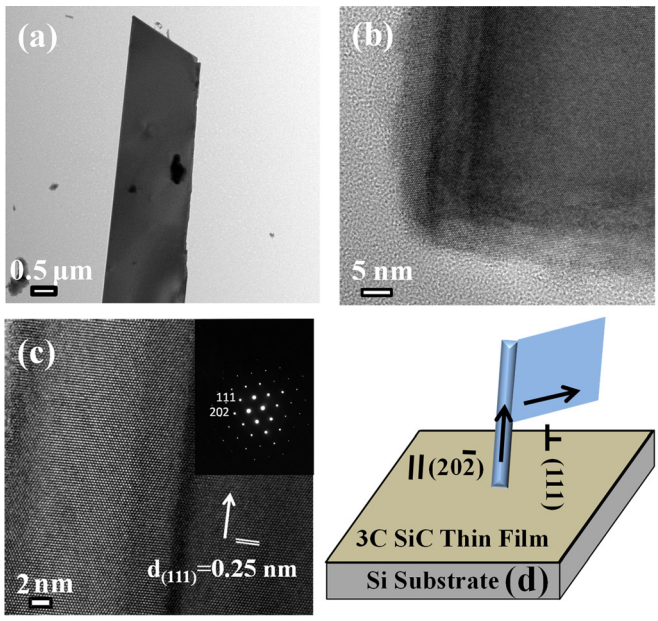

FIG. 5. (Color online) (a) TEM image of a single Ga_2O_3 nanosheet. (b) HRTEM image of the Ga_2O_3 nanosheet taken along the edge. (c) HRTEM image of the Ga_2O_3 nanosheet clearly showing the lattice fringes. Inset shows the SAED pattern of the nanosheet taken along the [10–1] zone axis. (d) Schematic illustration showing the growth directions of Ga_2O_3 nanorod and nanosheet.

Raman spectroscopy is a powerful technique to study the structural characteristics of the material. To differentiate Raman signals from nanorods and only focus on Raman modes from nanosheet, β-Ga_2O_3 nanostructures are first transferred onto the flat SiO_2-on-Si substrate. After that, the 532 nm Raman excitation laser is solely focused on the nanosheet region and the measurement position is indicated using a green circle in Fig. 6 inset. As shown in Fig. 6, eight major Raman active modes around 143.3 (B_g), 167.3 (A_g), 199.7 (A_g), 346.5 (A_g), 416.62 (A_g), 631 (A_g), 652.5 (B_g), and 767.7 (A_g) cm^{-1} are clearly visible in the measured spectrum. The peak located at ~520.5 cm^{-1} corresponds to Si TO mode. The Raman modes for the nanosheets are negligibly redshifted compared to the bulk Raman modes. The presented Raman results exhibit less shift as compared to those reported previously.[28–30] Rao *et al.* reported a blue shift of 10–40 cm^{-1} for Ga_2O_3 nanowires grown along the [110] crystallographic direction as compared to bulk Ga_2O_3.[28] The blue shift of the Raman modes was ascribed to growth direction induced internal strains in the nanowires. In contrast, Gao *et al.* reported a red shift of 4–23 cm^{-1} for their Ga_2O_3 nanorods.[29] They attributed the red shift of the Raman peaks to the presence of twin and edge dislocations in the nanorods. In our study, we have found a red shift of the Raman modes which is very small in comparison to previous reports. This indicates that the structural quality of the as synthesized nanosheets in terms of strain and defect levels is superior as compared to similar nanostructures reported in the literature by other groups.

The bending and straining test of an individual nanosheet is performed by a tungsten needle inside a SEM chamber. Figure 7 shows the sequential images of a representative Ga_2O_3 nanosheet under strain. The states of the nanosheet before and after applying strain are shown in Figs. 7(b) and 7(f), respectively. When the tungsten needle

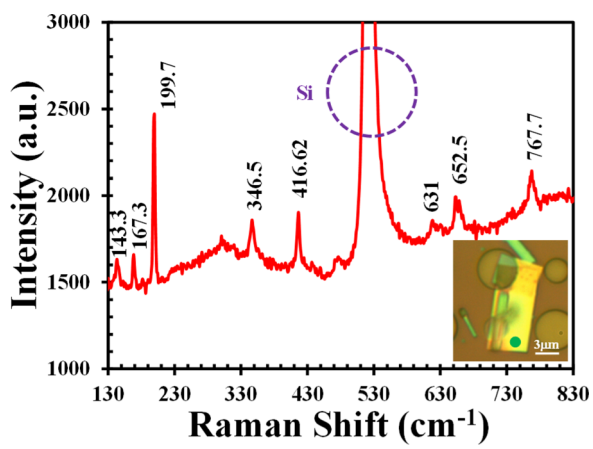

FIG. 6. (Color online) Micro Raman spectrum of a single Ga_2O_3 nanosheet transferred on a SiO_2-on-Si substrate. Inset shows the position on the nanosheet where the spectrum was taken.

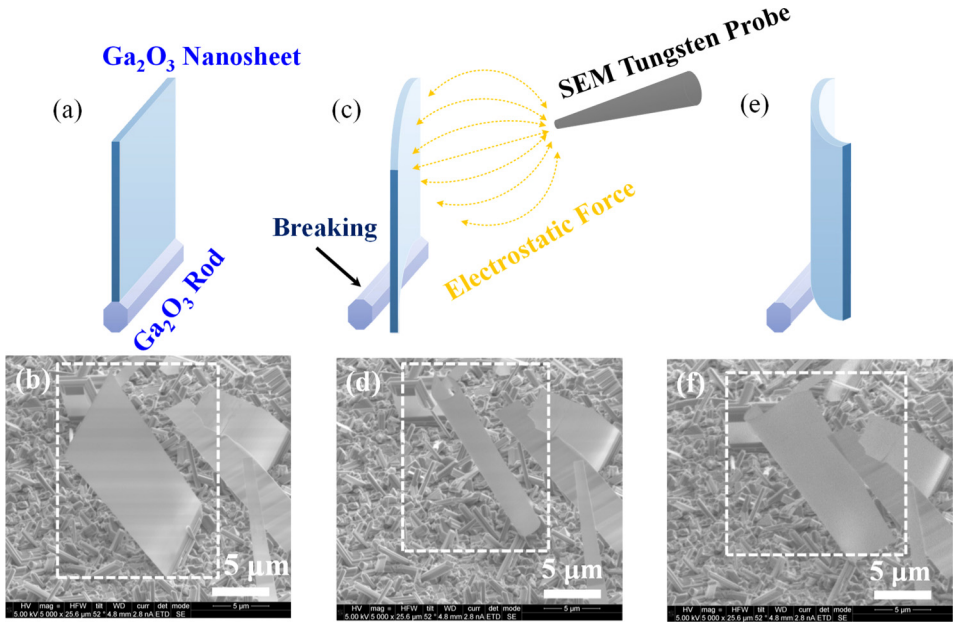

FIG. 7. (Color online) [(a), (c), (e)] Schematics of the experimental set up for a Ga_2O_3 nanosheet bending process inside an SEM. [(b), (d), (f)] Sequentially tilted FESEM images showing the bending of the Ga_2O_3 nanosheet under strain.

gradually approaches to Ga_2O_3 nanosheet, trapped charges from SEM field emission generate considerable electrostatic force between the nanosheet and the needle, straining it even before physical contact to the individual nanosheet [Fig. 7(c)]. During straining testing, interface between nanorod and nanosheet break when the nanosheet starts bending [Figs. 7(c) and 7(d)]. After straining from electrostatic force, the nanosheet has deformed elastically [Figs. 7(e) and 7(f)]. The nanosheet showed excellent mechanical flexibility compared to its bulk counterpart. The nanosheet recovered to its original flat shape after the removal of the strain. Since flexural rigidity is proportional to the cube of the thickness, a Ga_2O_3 nanosheet of 44 nm thickness has ~11 orders of magnitude smaller flexural rigidity than that of the bulk Ga_2O_3 (thickness ~200 μm). This kind of flexural rigidity has also been reported previously for Ga_2O_3 nanobelts and nanoribbons.[31,32] The unique mechanical properties of the Ga_2O_3 nanosheet make it an attractive potential candidate for nanoscale mechanically active devices and transducers applications.

IV. CONCLUSION

In summary, sizable two-dimensional β-Ga_2O_3 nanosheets have been synthesized on 3C-SiC-on-Si substrates by catalyst-free low pressure chemical vapor deposition. The nanosheets have a width range of ~1.5–7 μm and thickness range of ~20–140 nm. The single crystalline nature and the monoclinic structure of the nanosheets were verified by TEM, SAED patterns, and Raman spectroscopy. It has been found that the nanosheets originated from the sidewalls of Ga_2O_3 nanorods. It appears that the possible growth mechanism of the nanosheets is vapor-solid. These phase-pure and defect-free nanosheets are potential candidates for future functional nanodevices.

ACKNOWLEDGMENTS

Part of the material characterization was performed at the Swagelok Center for Surface Analysis of Materials (SCSAM) at CWRU. X.-Q. Zheng acknowledges partial support from a ThinkEnergy Fellowship.

[1]S. Kumar, C. Tessarek, G. Sarau, S. Christiansen, and R. Singh, Adv. Eng. Mater. **17**, 709 (2015).
[2]S. Rafique, L. Han, and H. Zhao, Phys. Status Solidi A **213**, 1002 (2016).
[3]S. Rafique, L. Han, M. J. Tadjer, J. A. Freitas, Jr., N. A. Mahadik, and H. Zhao, Appl. Phys. Lett. **108**, 182105 (2016).
[4]S. Rafique, L. Han, A. T. Neal, S. Mou, M. J. Tadjer, R. H. French, and H. Zhao, Appl. Phys. Lett. **109**, 132103 (2016).
[5]H. Okumura, M. Kita, K. Sasaki, A. Kuramata, M. Higashiwaki, and J. S. Speck, Appl. Phys. Express **7**, 095501 (2014).
[6]D. Gogova, G. Wagner, M. Baldini, M. Schmidbauer, K. Irmscher, R. Schewski, and Z. Galazka, J. Cryst. Growth **401**, 665 (2014).
[7]T. Oshima, N. Arai, N. Suzuki, S. Ohira, and S. Fujita, Thin Solid Films **516**, 5768 (2008).
[8]S. Kumar and R. Singh, Phys. Status Solidi RRL **7**, 781 (2013).
[9]S. Kumar, G. Sarau, C. Tessarek, M. Y. Bashouti, A. Hahnel, S. Christiansen, and R. Singh, J. Phys. D: Appl. Phys. **47**, 435101 (2014).
[10]S. Phumying, S. Labauyai, W. Chareonboon, S. Phokha, and S. Maensiri, Jpn. J. Appl. Phys., Part 1 **54**, 06FJ13 (2015).
[11]G. Wang, J. park, X. Kong, P. R. Wilson, Z. Chen, and J.-H. Ahn, Cryst. Growth Des. **8**, 1940 (2008).
[12]H.-S. Chung, S. C. Kim, D. H. Kim, J. W. Kim, O.-J. Kwon, C. Park, and K. H. Oh, J. Korean Phys. Soc. **55**, 68 (2009).
[13]S. Ohira, T. Sugawara, K. Nakajima, and T. Shishido, J. Alloys Compd. **402**, 204 (2005).
[14]S. Thirumala, K. Girija, V. R. Masteralo, and N. Ponpandian, J. Mater. Sci.: Mater. Electron **26**, 8652 (2015).
[15]B. Piccione, R. Agarwal, Y. Jung, and R. Agarwal, Philos. Mag. **93**, 2089 (2013).
[16]L. Gundlach and P. Piotrowiak, J. Phys. Chem. C **113**, 12162 (2009).
[17]S.-Y. Chen *et al.*, Phys. Chem. Chem. Phys. **15**, 2654 (2013).
[18]C. E. Kendrick, H. P. Yoon, Y. A. Yuwen, G. D. Barber, H. Shen, T. E. Mallouk, E. C. Dickey, T. S. Mayer, and J. M. Redwing, Appl. Phys. Lett. **97**, 143108 (2010).

[19]K. K. Cho, G. B. Cho, K. W. Kim, and K. S. Ryu, Phys. Scr. **T139**, 014079 (2010).
[20]S. Y. Park, S. Y. Lee, S. H. Seo, D. Y. Noh, and H. C. Kang, Appl. Phys. Express **6**, 105001 (2013).
[21]G. Sinha, A. Datta, S. K. Panda, P. G. Chavan, M. A. More, D. S. Joag, and A. Patra, J. Phys. D: Appl. Phys. **42**, 185409 (2009).
[22]F. R. Wong, A. A. Ali, K. Yasui, and A. M. Hashim, Nanoscale Res. Lett. **10**, 233 (2015).
[23]S. Rafique, L. Han, C. A. Zorman, and H. Zhao, Cryst. Growth Des. **16**, 511 (2016).
[24]H. Abderrazak and E. S. B. H. Hmida, *Properties and Applications of Silicon Carbide*, edited by R. Gerhardt (In Tech, Rijeka, Croatia, 2011), Chap. 16, p. 361.
[25]C. A. Zorman, S. Rajgopal, A. X. Fu, R. Jezeski, J. Melzak, and M. Mehregany, Electrochem. Solid-State Lett. **5**, G99 (2002).
[26]S. Rafique, L. Han, and H. Zhao, Cryst. Growth Des. **16**, 1654 (2016).
[27]C.-L. Kuo and M. H. Huang, Nanotechnology **19**, 155604 (2008).
[28]R. Rao, A. M. Rao, B. Xu, J. Dong, S. Sharma, and M. K. Sunkara, J. Appl. Phys. **98**, 094312 (2005).
[29]Y. H. Gao, Y. Bando, T. Sato, Y. F. Zhang, and X. Q. Gao, Appl. Phys. Lett. **81**, 2267 (2002).
[30]H. Z. Zhang *et al.*, Solid State Commun. **109**, 677 (1999).
[31]R. Zou, Z. Zhang, Q. Liu, J. Hu, L. Sang, M. Liao, and W. Zhang, Small **10**, 1848 (2014).
[32]M.-F. Yu, M. Z. Atashbar, and X. Chen, IEEE Sens. J. **5**, 20 (2005).